THIN FILMS

THIN FILM MATERIALS

Thin film ferroelectric materials and hexagonal piezoelectric materials are essential for fabrication of electronic and/or photonic devices. Historically ferroelectric materials were discovered in a form of bulk single crystals of Rochelle salt in 1920. Since then, a number of ferroelectric materials including $NH_4H_2PO_4$ (ADP), KH_2PO_4 (KDP), $LiNbO_3$ (LN), $LiTaO_3$ (LT), $BaTiO_3$ (BT), $PbTiO_3$ (PT), and $Pb(Zr,Ti)O_3$ (PZT) were developed in a form of bulk single crystals or bulk ceramics. Among these ferroelectric materials, perovskite (ABO_3) with oxygen octahedral structures has become an important ferroelectric material.

Ferroelectric materials are dielectrics that have a spontaneous polarization with nonlinear hysteretic properties and

J. Webster (ed.), *Wiley Encyclopedia of Electrical and Electronics Engineering*. Copyright © 1999 John Wiley & Sons, Inc.

Table 1. Ferroelectric Thin Films and Devices

Function	Devices: Materials	Miscellaneous
Ferroelectricity	FEDRAM:PZT, PLZT FESRAM: BPZT, SBT FEMFET:BMF	Nonvolatile High Ps, Pr PZT $>$ 20 μm/cm^2
High Permittivity	Capacitor for high count DRAM: SBT, ST, PZT, PLT	High permittivity PZT: 500–2000
Pyroelectricity	IR detector: PT, PLT	Sensitive/low noise PLT: $\gamma = 5.5 \times 10^{-4}$ C/m^2 K
Piezoelectricity	BAW/SAW: ZnO, AlN Filter PZT, PLT Resonator Oscillator Delay line	High coupling for SAW ZnO/sapphire: $k^2 = 5\%$ High temperature stability ZnO/glass: TCD = 0
Electrostriction	Actuator: PLT, PZT, ZnO MEMS	High sensitive
Acousto-optics	Integrated optics: ZnO, LN Channel switch PLT, PLZT Modulator	Low working voltage High-speed operation
Electro-optics	Integrated optics: LT, LN, BTO Coupler PLT, PLZT Channel switch Modulator Optical shutter EO disk memory	Pockels effect (linear EO) LN, LT, BTO, PLZT Kerr effect (quadratic EO) PLT, PLZT: $R = 1 \times 10^{-16}$ m^2/V^2 (6328 Å)

BPZT: $BaTiO_3$—$PbZrO_3$; SBT: $SrBi_2Ta_2O_9$, BST: $(Ba,Sr)TiO_3$; BTO: $Bi_4Ti_3O_{12}$; LN: $LiNbO_3$; LT: $LiTaO_3$; BMF: $BaMgF_4$

show several unique properties including high dielectric permittivity, high piezoelectricity, high pyroelectricity, and high electro-optic characteristics.

Bulk ferroelectric materials were widely used to manufacture discrete electronic components including ceramics capacitors, band pass filters, resonators, ultrasonic transducers, and positive temperature coefficient (PTC) thermistors. Novel ferroelectric materials such as optical transparent ferroelectric $(Pb,La)(Zr,Ti)O_3$ (PLZT) ceramics were developed by Haertling and Land in 1971. A high-speed electro-optical shutter was realized using hot-pressed transparent PLZT ceramics. The bulk-type ferroelectric devices, however, could not meet recent requirements of miniaturization and/or integration with Si and/or GaAs semiconductive devices.

Thin film ferroelectric materials have a high potential for miniaturization and/or integration with the semiconductive devices. Thin films are also important to the understanding of ferroelectricity. Thin films are commonly fabricated by depositing individual atoms on a substrate. The film thickness is typically less than several micrometers. The structure of thin films is essentially homogeneous on an atomic scale. Thin films exhibit the following useful aspects including thin film effects:

1. Unique materials properties resulting from the atomic scale growth
2. Size effects at ultrathin films
3. Unique functional properties at layered structure including human-made superlattice and tailored ferroelectric materials

Polycrystal and/or single-crystal thin films of ferroelectric/piezoelectric materials are used for the fabrication of thin film devices. The polycrystal thin films are commonly deposited on a noncrystalline substrate such as fused quartz, borosilicate glass, and passivated Si substrates. The single-crystal thin films are heteroepitaxially grown on a foreign single crystal substrate such as sapphire, MgO, $SrTiO_3$ (ST), $LaAlO_3$, and YSZ substrates. At the early stage, the ferroelectric thin films were considered to be a simple substitution of bulk dielectric materials by thin films, such as a fabrication of thin film discrete capacitor for an electronics system.

Since the 1970s, several kinds of thin film ferroelectric and/or piezoelectric films were developed for a fabrication of bulk acoustic wave (BAW) devices, surface acoustic wave (SAW) devices, thin film ferroelectric memory, acousto-optical (AO) devices, and electro-optical (EO) devices. Among these thin films, piezoelectric ZnO and CdS thin films of hexagonal structure were extensively studied for a fabrication of the thin film SAW devices and the thin film AO devices, although the piezoelectric hexagonal ZnO and/or CdS were not ferroelectric materials. The technology for a production of ZnO thin film SAW devices was established, and the ZnO thin film SAW devices are used in practice. Since the 1980s, much attention had been paid to the application of ferroelectric thin films such as PZT and $(Pb,La)TiO_3$ (PLT) to thin film optical waveguide devices, an integrated pyroelectric sensor, a memory capacitor of high dielectric permittivity at megabit dynamic random access memory (DRAM), the ferroelectric random access memory (FERAM) combined with Si and/or GaAs integrated circuits, and a thin film microactuator. Two-dimensional integrated optical devices are made by electro-optic thin films. The multilayer structures tailor SAW materials with designed acoustic velocity, electromechanical coupling, and temperature stability. The electromechanical coupling for the generation of SAW is enhanced at the layered structures.

High electromechanical coupling with zero temperature coefficient of delay time (TCD) could be achieved at the layered structure of ZnO/glass substrate. The electrostrictive properties are also of interest for making a microelectromechanical system (MEMS). A MEMS provides integration of sensors, actuators, and electronic circuits in a single chip. Table 1 shows typical thin film ferroelectric materials and their devices including hexagonal piezoelectric thin films (1–3).

THIN FILM FABRICATION

Thin films of ferroelectric materials are fabricated by a thin film deposition process including physical vapor deposition (PVD), chemical vapor deposition (CVD), and chemical solvent deposition as shown in Table 2.

Thin films of ferroelectric materials were first fabricated by Feldman in 1955 for $BaTiO_3$ by PVD using a simple vacuum evaporation. In the 1960s others tried to deposit thin films of $PbTiO_3$ by cylindrical magnetron sputtering. The controlled deposition of the perovskite ferroelectric materials of ABO_3 and $A(B1,B2)O_3$ structure could not be attained because of their complex chemical composition. Since the middle of the 1970s, rapid progress has been observed in the thin film deposition processes including planar magnetron sputtering, molecular beam epitaxy (MBE), and metal organic chemical vapor deposition (MOCVD). After the discovery of high-Tc superconductors of layered perovskite in 1986, rapid progress has been seen in the development of the deposition process for complex perovskite with atomically controlled crystal structure using sputtering, MBE, laser ablation, and MOCVD.

Typical configuration of deposition systems are shown in Fig. 1. A conventional thermal evaporation process provides inhomogeneous and nonstoichiometric thin films. A multisource MBE system is used for the deposition. The laser ablation is carried out by the direct evaporation of source ferroelectric materials resulting from the irradiation of high-intensity pulsed excimer laser. The mechanism of laser ablation includes photo and thermal evaporation. The pulsed evaporation by high-intensity laser improves the inhomogeneity and/or nonstoichiometry, although the laser ablation includes the thermal evaporation process. The phenomenon of sputtering consists of a nonthermal evaporation. The sputtering process essentially provides homogeneous and stoichiometric thin films of complex ferroelectric materials because the sputtering mechanism consists of removing source materials (target) on an atomic scale by an impact of energetic ions through the momentum transfer mechanism. Multitarget magnetron sputtering is used for the deposition of layered structures and/or human-made superlattices. The sputtering process has a high potential for the fabrication of complex ferroelectric thin films. In the plasma-assisted MOCVD, energetic electron in gas plasma enhances the chemical reaction. At present these thin film processes provide the thin films of perovskite with an accuracy of 1 nm corresponding to two or three of their crystal units. The chemical solvent deposition provides a simple fabrication process. However, the deposited thin films are essentially porous because the growth process is governed by a conventional thick film technology including dipping and/or spinning of sol-gel precursor solution followed by annealing for sintering.

The deposition, chiefly by the sputtering, of transducer quality ZnO thin films has been studied since the 1970s. The

Table 2. Thin Film Deposition Process

Classification	Deposition System	Source Materials	Film Structure
Vapor phase deposition			
PVD	Thermal evaporation EB crucible MBE	Individual metals Individual oxides Multisource	Uniaxial crystal by epitaxial growth (poly/single)
	Laser ablation	FE compounds Individual oxides Multitarget	Tailoring FE by layer-by-layer deposition In situ poling
	Sputtering	FE compounds Individual metals Individual oxides Multitarget	
CVD	Low-pressure CVD MOCVD Plasma-assisted MOCVD	Individual halide Metal organic gas	Uniaxial crystal by epitaxial growth (poly/single) In situ poling
Chemical solvent deposition			
	MOD Sol-gel deposition	Individual Metal organic gas	Multiaxial (polycrystal) Ex situ poling (porous)

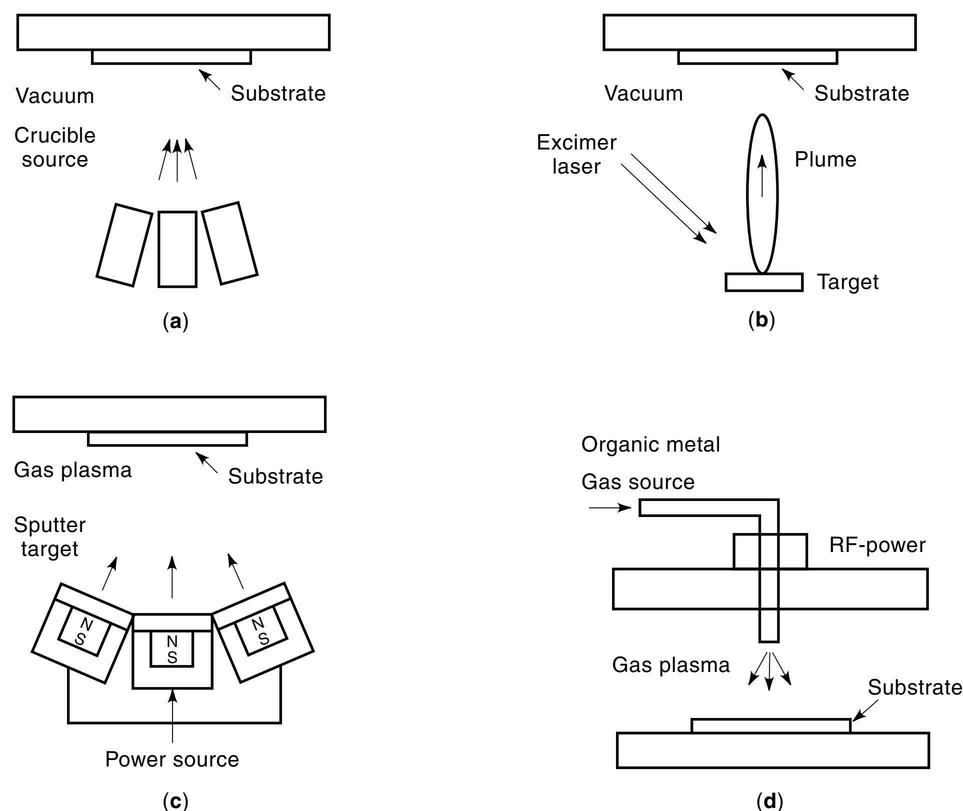

Figure 1. Typical configuration of thin film deposition systems: (a) multisource MBE, (b) laser ablation, (c) multitarget sputtering, (d) plasma-assisted MOCVD.

technology to fabricate ZnO thin films has already been established. The *c*-axis oriented polycrystalline thin films are deposited on a glass substrate by direct sputtering from the ZnO target. The *c*-axis orientation on the glass substrate is quite reasonable because the film growth of a hexagonal structure is governed by Bravis's empirical law for crystal growth, where the most densely packed plane (*c*-plane) will be the most preferable surface of crystal growth. Single-crystal ZnO thin films are epitaxially grown on a sapphire substrate. The *a*-axis-oriented ZnO thin films are epitaxially grown on *R*-plane sapphire.

It is particularly important to understand the structure of thin films because it can have a profound influence on the operation of the thin film devices.

Thin films of polycrystalline phase comprise a column geometry with an interfacial layer between the thin films and a substrate. Low dielectric permittivity of the interfacial layer apparently reduces the permittivity of the ferroelectric thin films and/or increases a coercive field (extrinsic thickness effect). The decrease of dielectric permittivity for ferroelectric thin films with the decrease of their film thickness is also governed by the depolarization phenomenon (intrinsic thickness effect).

The epitaxial ferroelectric thin films show different microstructures depending on the degree of lattice match between the thin films and substrates. It is generally believed that, under an excellent lattice match, the thin films such as PT on ST show a single domain; under a poor lattice match for both *a*- and *c*-axes the thin films such as PT on MgO show a multiaxial crystal structure; and under a fairly good lattice match the thin films such as PT on $KTaO_3$ (KTO) constitute a periodic domain structure. These microstructures are grown primarily to minimize the total energy of the heterostructure. The phenomena are understood by linear-elasticity theory and a Landau-Ginzburg Devonshire type phenomenological theory.

The actual epitaxial thin films of ferroelectric materials commonly constitute inhomogeneous microstructures including an interfacial layer that resembles polycrystalline thin films on a glass substrate as a result of the inhomogeneous nucleation at the initial-stage of film growth. A selection of

Table 3. Lattice Parameters of Typical Single-Crystal Substrates

	Crystal System	Structure	Lattice Constant (Å)	Coefficient of Expansion (10^{-6}/K)
Sapphire	Trigonal	Corundum	a = 4.763	7.5–8
MgO	Cubic	NaCl	a = 4.203	13.8
$SrTiO_3$	Cubic	Perovskite	a = 3.905	10.8
$LaAlO_3$	Pseudo cubic	Perovskite	a = 3.792	10
YSZ	Cubic	Fluoride	a = 5.16	10
$KTaO_3$	Cubic	Perovskite	a = 3.989	6.7
$PbTiO_3$	Tetragonal	Perovskite	a = 3.889	16.1
			c = 4.1532	−54.2
	Cubic		a = 3.961	

epitaxial relations:
(111)PT//(001)sapphire
(100)PT//(100)ST
(100)PLZT//(100)MgO
(111)PLZT//(0001)sapphire
(100)PLZT//(100)ST
(0001)ZnO//(0001)sapphire
$(11\bar{2}0)$ZnO//$(01\bar{1}2)$sapphire (*R*-plane)
(0001)LN//(0001)sapphire
(0001)LN//(0001)LT

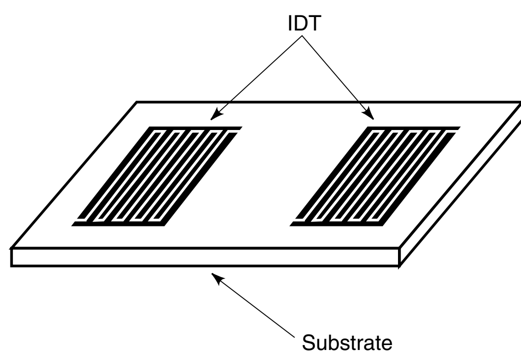

Figure 2. Interdigital transducer formed on the surface of the piezoelectric substrate.

substrate materials is important for the control of thin film growth. Typical structural properties of substrates are shown in Table 3 (4–6).

THIN FILM DEVICES

Thin Film SAW Devices

The use of thin film SAW devices is an example of a successful application using piezoelectricity of hexagonal thin films and perovskite ferroelectric thin films. In the quasi-static approximation, the acoustic fields associated with plane waves in a piezoelectric medium are obtained by solving the stiffened Christoffel equation. In the case of a half-space medium with a free boundary surface, the boundary conditions must be satisfied and the mechanical stress and electric displacement must be calculated from the piezoelectric constitutive equations. These procedures give the solution as a SAW, which acoustic vibration energy concentrates near the surface of elastic solid materials. The Rayleigh wave and Love wave are obtained as the typical solutions of SAWs. The particle displacement of the former is in the sagittal plane, which is perpendicular to the surface and parallel to the wave-propagation direction, and that of the latter is parallel to the surface

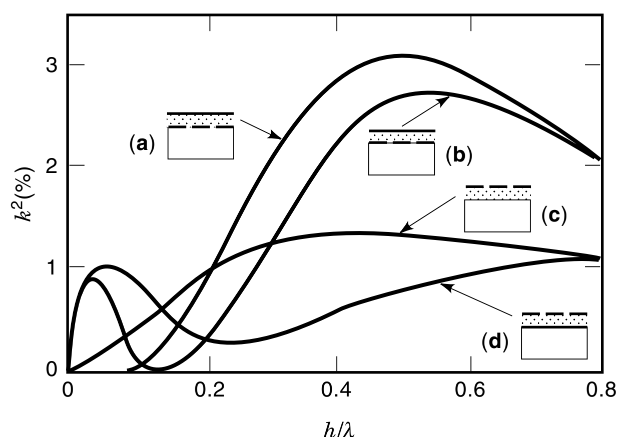

Figure 3. Calculated result of an effective electromechanical coupling constant k^2 for each configuration in the case of *c*-axis-oriented ZnO film on fused quartz. Four types of thin film electrode configurations are illustrated (7).

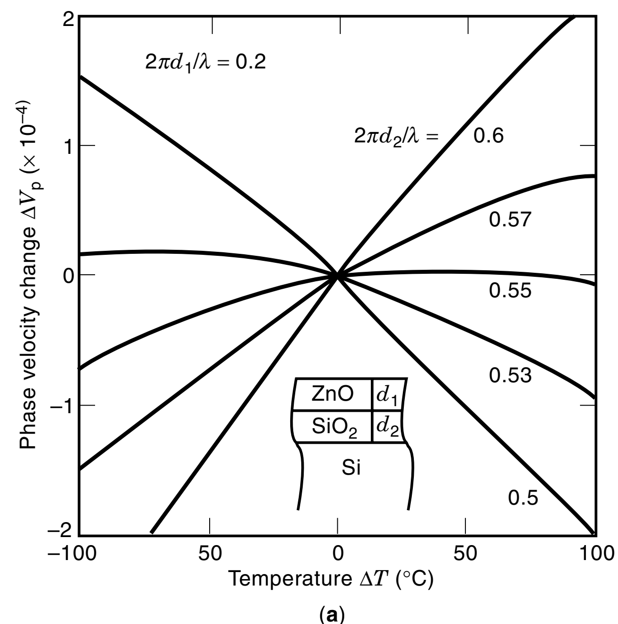

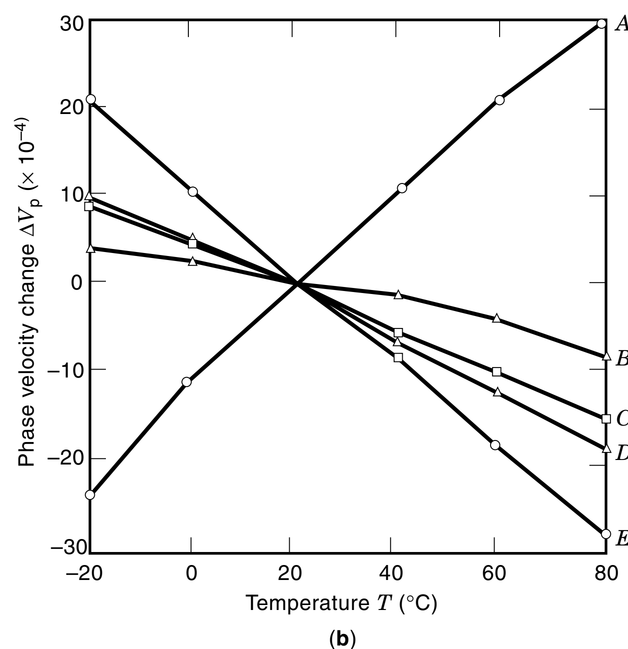

Figure 4. Temperature deviation of the center frequency of the SAW IDT constructed by the ZnO thin film: (a) the SiO_2 or fused quartz layer and the Si substrate; (b) the borosilicate-glass substrate (9).

and perpendicular to the direction of propagation. The SAW makes possible acoustoelectronic devices including the SAW filter for cellular phone/PCS/pager.

Generation of SAWs. The SAW modes can be generated by an interdigital transducer (IDT) formed on the surface of the piezoelectric substrate shown in Fig. 2. In the bulk SAW devices, bulk single crystals such as the $LiNbO_3$ and/or $LiTaO_3$ are adopted as the piezoelectric substrate. Whereas in the thin film SAW devices, a layered structure consisting of a piezoelectric thin film on the nonpiezoelectric mediums is used

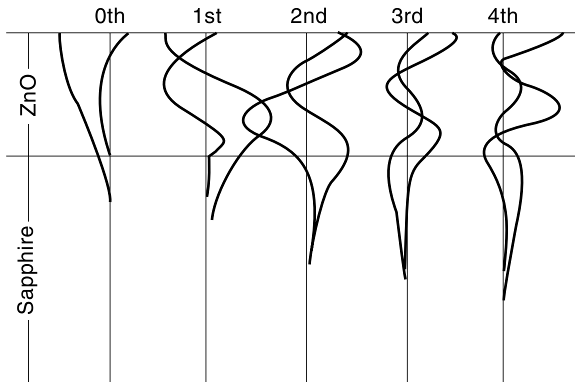

Figure 5. Depth profiles of the particle displacement in the sagittal plane for the fundamental mode and higher four modes of the Rayleigh-type wave.

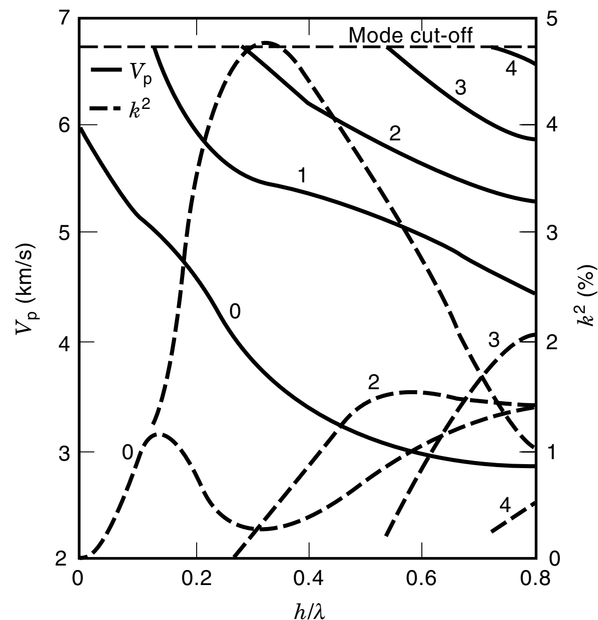

Figure 6. Rayleigh-type and Love-type wave mode solutions as a function of h/λ on the [1000] direction of the single crystal $(11\bar{2}0)$ ZnO thin film epitaxially grown on the $(01\bar{1}2)$ sapphire surface. Solid lines and broken lines show the phase velocity V_p and the effective coupling coefficient k^2 (17).

as the piezoelectric substrate. Figure 3 shows the calculated result of an effective electromechanical coupling constant k^2 for four types of electrode configurations of a c-axis-oriented ZnO film on fused quartz. These electrode configurations for a thin film SAW transducer are also illustrated in Fig. 7. Each configuration consists of an IDT with or without a counter electrode. The value of k^2 is determined by the relation $k^2 = \Delta V_p/V_p$ where ΔV_p is the variation of SAW phase velocity V_p by the short condition of the surface electric field. The k^2 is simply evaluated by the equation $k^2 = \pi\omega_0 C_T/4NG_a$, the in-line model of Smith's equivalent circuit model for electromechanical bulk wave, where ω_0, C_T, G_a, and N are the synchronous frequency, capacitance, radiation conductance, and number of finger pairs of IDT, respectively. The in-line model (the major electric field component is parallel to the surface) becomes almost equal to the crossed-field model (the major electric field component is perpendicular to the surface) under the rough condition of $k^2N > 1$. Figure 3 shows that k^2 varies with the ZnO film thickness, and the variations show a double-peaked character for the IDT structures including the counter electrodes. Note that the k^2 for thin films is higher than the bulk value at optimum film thickness.

Temperature Stability. SAW-layered structures have flexibility in that substrate materials can be chosen to adjust the temperature coefficient of a center frequency (TCF) and a delay time (TCD). The temperature stability of TCF or TCD is given by the equation, $(1/f)(dt/dT) = (1/t)(dt/dT) = (1/v)(dv/dT) - \beta$, where β denotes the thermal expansion coefficient of the substrate. The tendency of the phase velocity change $(1/v)(dv/dT)$ varies with the layered film thickness and elastic properties of the substrate materials. A suitable film thickness and a pertinent selection of substrate materials result in a zero TCD. Figure 4(a) shows one example of such a temperature deviation of the center frequency of the SAW IDT, which consists of the ZnO thin film, the SiO_2 or fused quartz layer, and the Si substrate. In this structure, the TCF of ZnO has a negative value of about −30 ppm/°C, and that of fused quartz has a positive value of +60 ppm/°C. These opposite values cancel the TCF while controlling the thickness of the SiO_2 layered film. Another example is shown in Fig. 4(b). Here the borosilicate-glass substrate can control TCF by controlling the composition ratio of the elements added to the glass.

SAW in Layered Media. The Rayleigh wave and Love wave are the solutions for a half-space medium with a free boundary surface. In layered structures, which include the thin plate rigidly bonded to the half-space (or substrate) having different material properties, the solutions for propagating waves must satisfy the appropriate wave equation in the layer and in the substrate as well as the boundary conditions imposed by the interface and the free surface. We know that fundamental and higher-order modes of both Rayleigh and

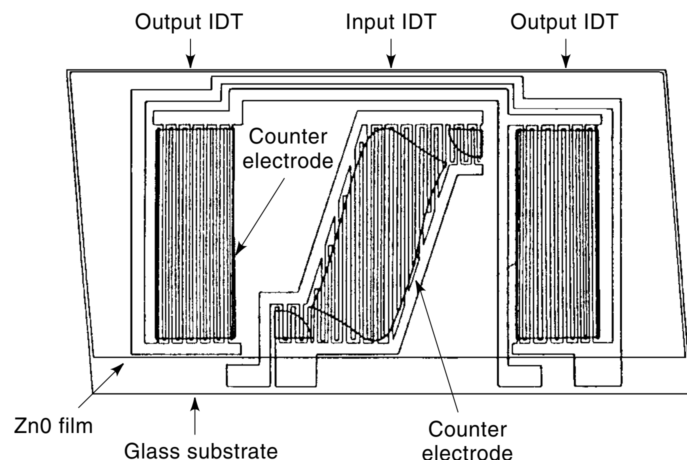

Figure 7. IDT configuration of SAW VIF filters with two normal output IDTs and one apodized input IDT on the layered substrate.

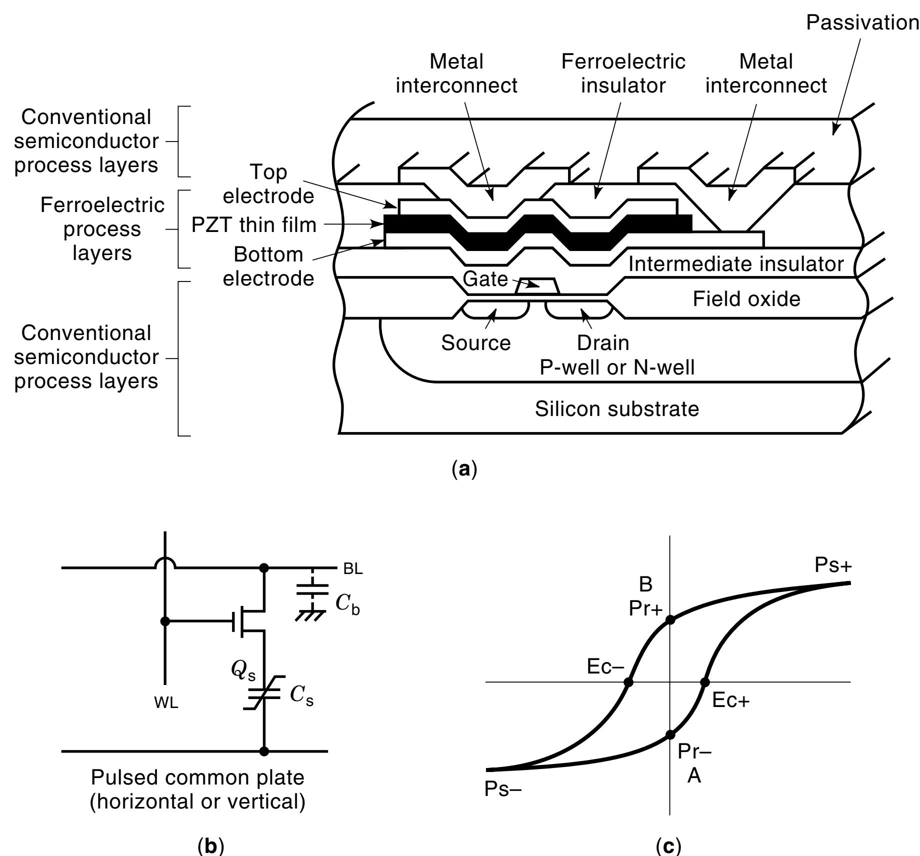

Figure 8. (a) Cross-sectional view of FE-DRAM with (b) a schematic circuit and (c) a hysteresis loop of ferroelectric thin films [Ramtron Corp. (4)].

Love waves can propagate when the bulk shear wave velocity of the layer is lower than that of the substrate. This condition corresponds to that of the heavier and less stiff layer loads on the substrate and will tend to confine the propagation energy to the layer. In this case, the propagating wave nodes are regarded as the modified plate modes. Sezawa discovered that a second fundamental mode may also exist in layered media. The Rayleigh modes and Sezawa modes correspond to symmetric and antisymmetric modes of a free plate modified by the contact of the surface with the substrate. In addition to these, the layer on an infinite half-space is open on one side, and there is a possibility of radiation or energy leakage out of the layer into the half-space. This condition gives the leaky wave solution for SAW.

The particle displacement of the SAW in the sagittal plane degrades with the depth from the surface. Also in the case of the layered substrate, almost the same situation exists in the half-space substrate. However, the degradation of that area in or near the top layer is different from the monotonous degradation of the zeroth Rayleigh mode. The amplitude distribution of the particle displacement is calculated for each propagating mode. Figure 5 shows the depth profiles of the particle displacement in the sagittal plane for the fundamental mode and higher four modes of the Rayleigh-type wave. More complex profiles and deeper penetration are shown for the particle displacement of higher-order modes. Moreover, Fig. 5 shows that the higher-order modes have a large displacement component in the substrate. So, it can be understood qualitatively that the higher-order modes have a higher phase velocity because the phase velocity of the substrate is higher than that of the layer.

In Fig. 6, the solid lines and broken lines show the phase velocity V_p and the effective coupling coefficient k^2 of the Rayleigh-type and Love-type wave modes as a function of h/λ, respectively, where h is the layer thickness. These numerical results were obtained for the SAW directed to [1000] ZnO axes in the layered structure with the ZnO layer on the R-plane sapphire substrate. The first mode of the Rayleigh-type (zero Sezawa mode) shows an exceedingly large maximum value of k^2 with very high phase velocity at relatively small h/λ. These computer solutions were experimentally confirmed. For higher Rayleigh-type modes, responses were still

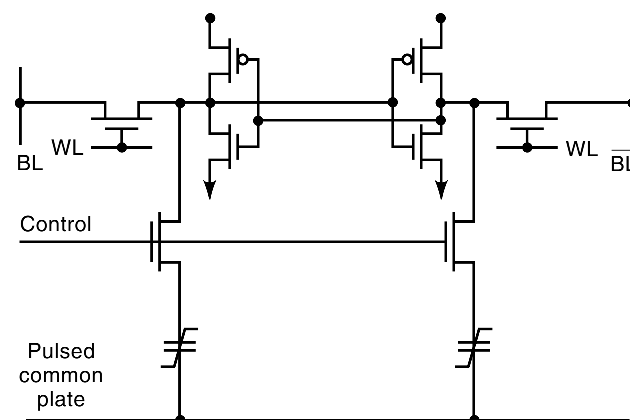

Figure 9. Schematic circuit of 256-bit FESRAM [Ramtron Corp. (18)].

Type	Conventional ceramics ($PbTiO_3$)	New thin film (*c*-axis oriented PLT)
Structure	Electrode Grain Domain 300 μm Electrode	Self-polarization Electrode PLT thin film Electrode Substrate Single crystal
Pyroelectric coefficient γ	1.8×10^{-8} [C/cm^{2}K]	5.5×10^{-8} [C/cm^{2}K]
Figure of merit F_m	4.4×10^{-9} [Ccm/J]	14×10^{-9} [Ccm/J]
Merits		High S/N (× 10) High responsivity Small size

Figure 10. Structure and pyroelectric properties of La-doped PT (PLT) thin films and conventional bulk PT ceramics (21).

observed above the mode cut-off frequency as leaky mode responses.

Thin Film SAW Filters. Thin film SAW devices are constructed by the thin film IDTs on nonpiezoelectric substrates, by high-frequency propagation of the higher-order modes of layered SAW, the substrate selected for the temperature stability, and so on. These distinguishing characteristics can realize the high performance of band-pass filters, resonators, delay lines, convolvers, integrated devices, and acousto-optic devices. The video intermediate frequency (VIF) filters for color TV sets were the first thin film mass-production devices. The frequency range of a VIF filter of 50–60 MHz is low enough for the SAW propagation loss of polycrystalline piezo-

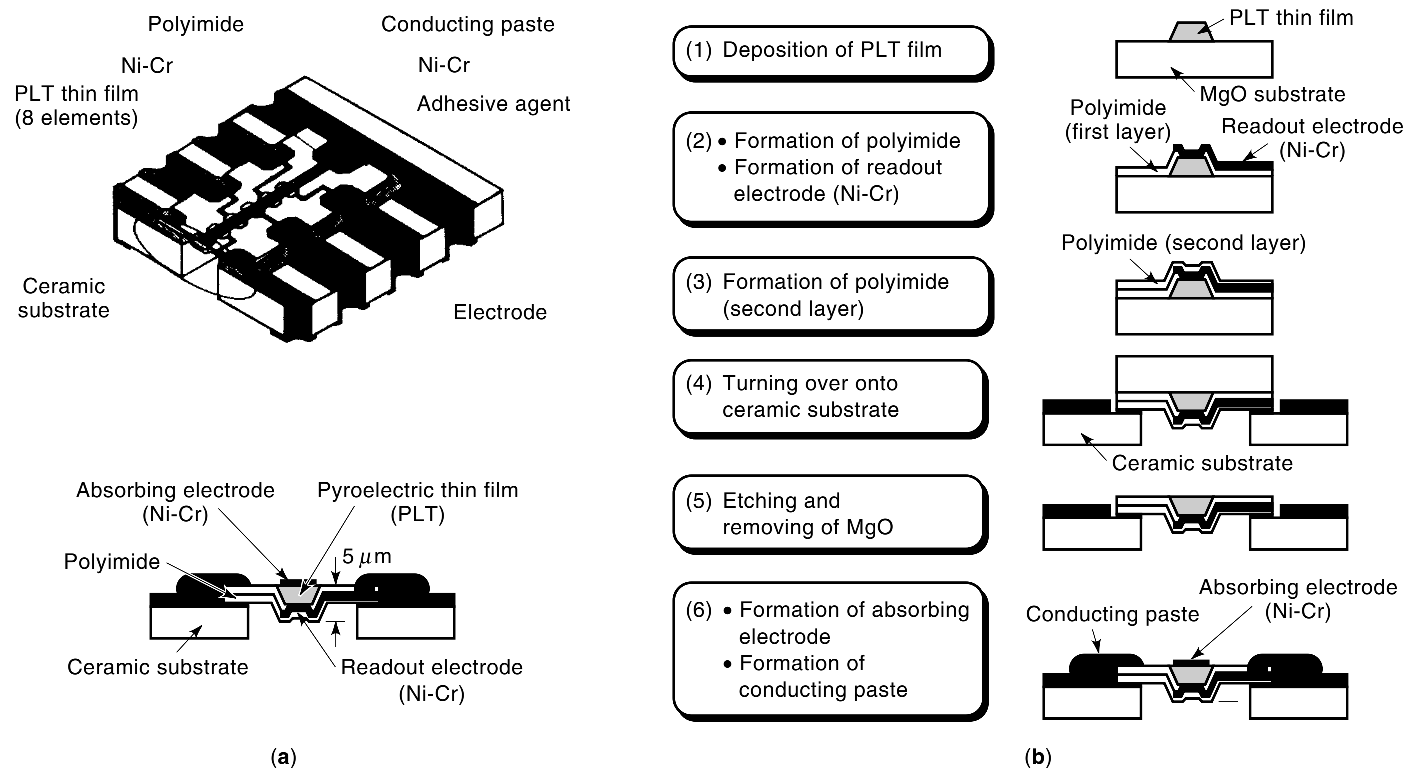

Figure 11. Schematic configuration of a linear array IR sensor for (a) a smart air conditioner and (b) its fabrication process (21).

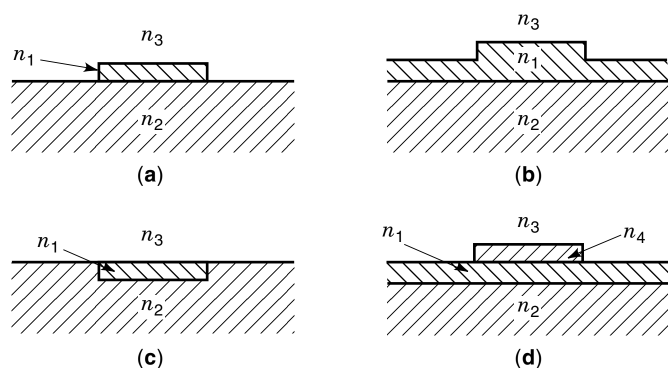

Figure 12. Cross-sectional view of thin film optical channel waveguide: (a) raised-strip type, (b) ridge type, (c) embedded type, and (d) strip-loaded type. n_1, n_2, n_3, n_4 are refractive index of waveguide, substrate, environment, and loded strip, respectively.

electric thin films such as *c*-axis-oriented ZnO films on a borosilicate-glass substrate. The thin film SAW filter shows excellent long-term stability. The long-term drift of the center frequency is less than 100 ppm after 1000 hours of exposure to 125°C in the air. The long-term stability of the ZnO thin film SAW filter is higher than that of bulk single-crystal $LiNbO_3$ SAW filters because of the absence of subsurface damage inflicted during sawing and polishing, which is unavoidable for bulk SAW devices. Figure 7 shows one example of the configuration of SAW VIF filters with two normal output IDTs and one apodized input IDT.

Another example is the high-frequency filter of epitaxially grown single-crystal thin film, which has low propagation loss of higher-order Rayleigh wave modes in the gigahertz range. The ZnO single crystal film on sapphire substrate is the typical construction of devices which provide 4.37 GHz filters with a phase velocity of 5327 m/s and an insertion loss of 16 dB by 0.27 μm thick ZnO film, 3-IDT of 50 nm thick Al electrodes, and third-order response of double electrode type IDTs. These excellent properties of thin film SAW filters are able to provide the high performance of information communication systems (7–17).

Ferroelectric Nonvolatile Memory

The basic operation of ferroelectric nonvolatile memory is switching of polarization states in a ferroelectric ABO_3 structure. Figure 8 shows a typical configuration and schematic circuit of ferroelectric nonvolatile memories, dynamic random

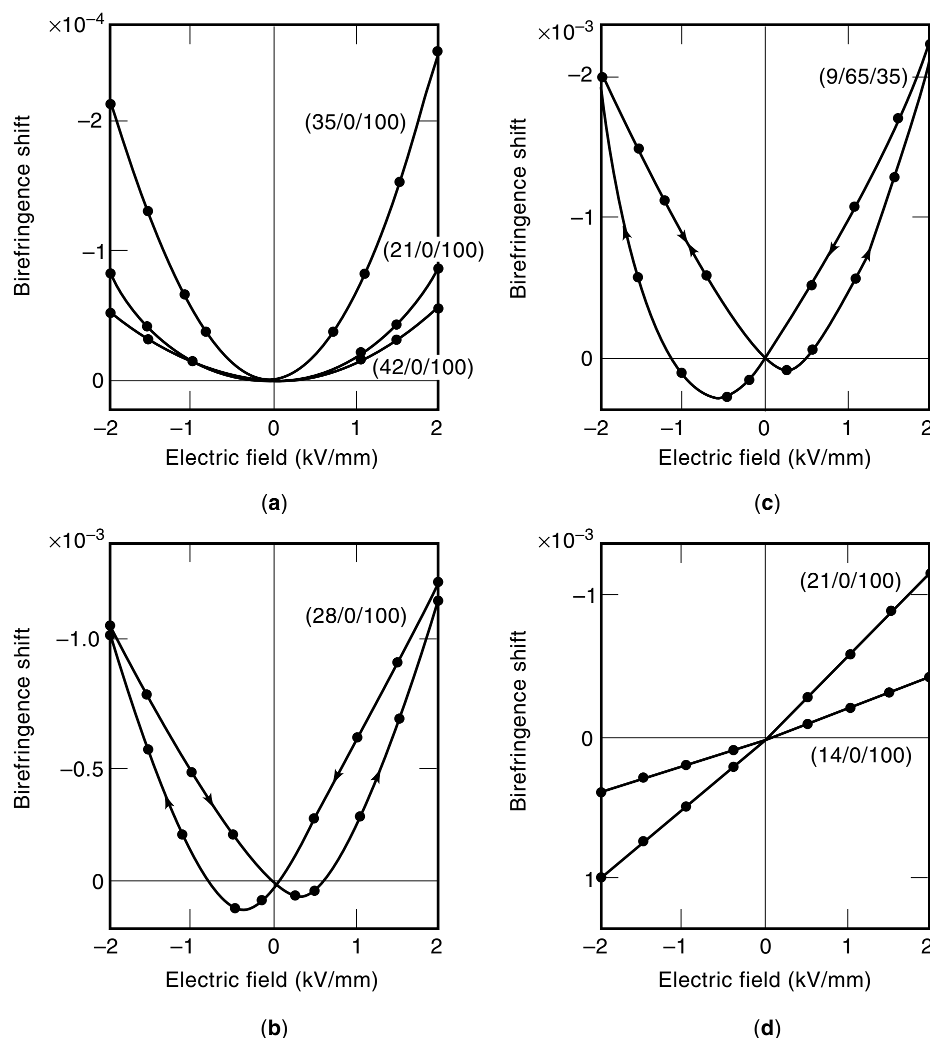

Figure 13. The effective birefringence shift as a function of transverse electric field for PLZT thin film of 0.4 mm in thickness (23).

access memory (FEDRAM). The FEDRAM resembles a conventional dynamic random access memory (DRAM). The memory capacitor C_s of DRAM is replaced by a ferroelectric thin film capacitor. The C_s is in series with a MOS (metal-oxide-semiconductor) transistor whose source is connected to the bit line, the gate to the word line, and the drain to the pulsed 5 V common plate. In the FEDRAM, the polarization of the ferroelectric thin films switches to the opposite polarity on application of an electrical field higher than the coercive force when the MOS transistor is turned on by the appropriate voltage on the gate. In the hysteresis loop of memory capacitor C_s, the position A is taken to be a bit 1 state and B, a bit 2 state. The switching signal is detected by the voltage change at the bit line V_b. The V_b is given by $V_b = Q_s/C_b$, where Q_s denotes change of charge at switching on the capacitor C_s, C_b denotes the storage capacitor at the bit line. The Q_s is given by $Q_s = 2P_r$, where P_r denotes remanent polarization for ideal ferroelectric thin films having a symmetric hysteresis loop. For memory capacitors, PZT thin films are widely used. The P_r is 20–30 μC/cm^2 for typical PZT thin films. The value of Q_s for each memory cell is 400–600 fC for a cell area of 1 μm^2 which is enough for the switch memory operation because the minimum detectable value of Q_s for each cell is 20–30 fC at the conventional DRAM. The switching speed is essentially governed by the switching time of polarization reversal. The switching time is 1 ns for typical ferroelectric materials. The FEDRAM has some definite advantages including a permanent memory and radiation hard characteristics. However, there are disadvantages of switch fatigue resulting from domain switching. Historically the ferroelectric memory was proposed in the first part of the 1970s and first developed in 1987 by Ramtron Corp., Colorado Springs, and Krysails Corp., Albuquerque. The first developed ferroelectric memories look like the six-transistor static random access memory (SRAM) except that they include an additional pair of ferroelectric thin film capacitors, as shown in Fig. 9. Presently, the FEDRAM with a single transistor, where the ferroelectric thin films make a conventional DRAM nonvolatile, has been extensively studied to improve long-term stability. The ferroelectric thin films placed in the gate area of a MOS transistor provide another type of ferroelectric memory—the ferroelectric memory field effect transistor (FEMFET). Depending on the polarization of the gate materials, the source-to-drain current is increased or decreased significantly. The 1 or 0 state is detected by monitoring the source-to-drain current without switching the remanent polarization. This type of switch gives a nondestructive read out. This type of memory is under research because the interface control between the ferroelectric thin film and semiconductor is not completed.

Apart from the FEDRAM, the high dielectric permittivity of ferroelectric films is used for the local capacitor in high-count DRAM to reduce the area of the memory capacitor and/or eliminate the complex trenching and/or corrugation structures for the increased capacitive area. The high permittivity of the ferroelectric thin films achieves the flat structure of the memory cell. In the mega-/gigabit DRAM, the requirement for ferroelectric thin films is a permittivity of 200–2,000 at a film thickness of 100 nm without remanent polarization. The ferroelectric thin films should be used above their Curie temperature. If ferroelectric thin films are used, their operating coercive field should be large (18,19).

Thin Film Pyroelectric Infrared Detectors

Ferroelectric materials have been used for making pyroelectric infrared detectors by measuring the pyroelectric current because they exhibit a large pyroelectric effect. The pyroelectric effect is described by the pyroelectric coefficients γ which relates the change of polarization to the change in temperature. Pyroelectric current i_p will be detected by the temperature change of the detector materials generated by absorbed infrared radiation. The i_p is given by $i_p = \gamma(dT/dt)$. Bulk ferroelectric single crystals TGS (triglycine-sulphate) and LT, ferroelectric polymer PVDF (polyvinyl-di-fluoride), and ferroelectric ceramics PT and $PbZrO_3$ (PZ) are widely used for making pyroelectric infrared detectors. The pyroelectric materials are evaluated by figures of merit; $F_1 = \gamma/C_v$, $F_v = \gamma/C_v \cdot \epsilon$, $F_M = \gamma/C_v\ (\epsilon \cdot \tan\ \delta)^{1/2}$, where C_v denotes a volume specific heat, ϵ denotes a dielectric constant, and F_1, F_v, and F_m denote the figure of merit related to a current response, an output voltage response, and a detectivity, respectively. Perovskite thin films of PT and/or PLT are epitaxially grown on a Pt-metallized MgO substrate. The MgO substrate is removed after deposition of perovskite thin films. The as-deposited thin films show a highly oriented structure, which results in excellent pyroelectric properties without poling treatment after de-

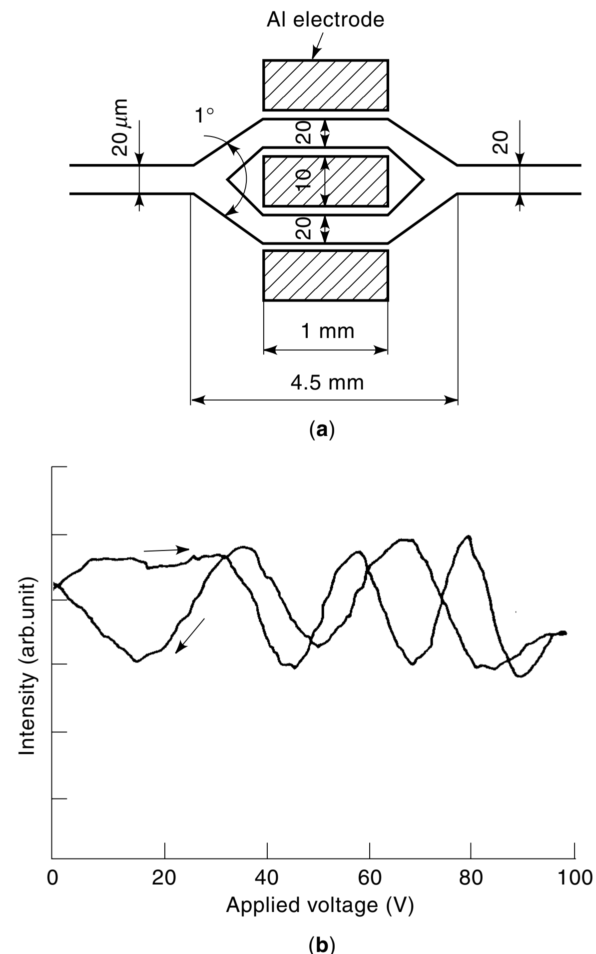

Figure 14. (a) Configuration of a thin film Mach–Zehnder interferometer using PLZT thin film on sapphire and (b) the variation of output light intensity with applied voltage (25).

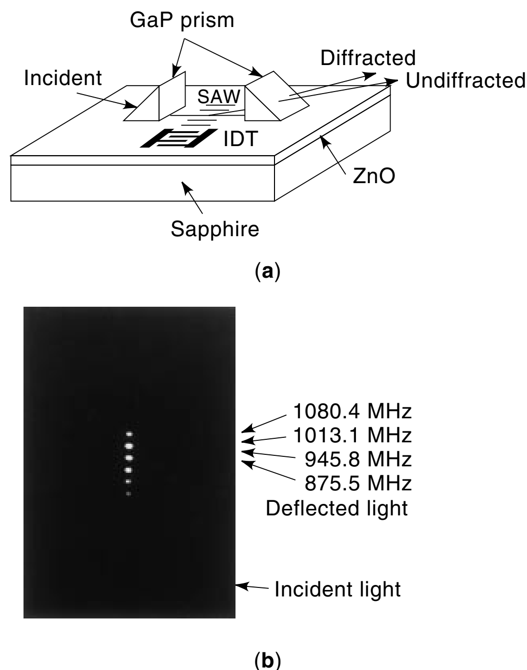

Figure 15. (a) Configuration of thin film AO Bragg deflector using ZnO thin film waveguide on sapphire and (b) a deflected light beam as a function of applied frequency at IDT driven by the first-order Sezawa mode of SAW (28).

position. The single-domain structure with a low dielectric constant in the c-axis direction improves the figure of merit of conventional ceramic pyroelectric materials. Figure 10 shows the typical pyroelectric properties of bulk and thin film PLT. The integrated infrared sensor array shown in Fig. 11 was created using thin film infrared detector technology. The sensor array, manufactured by Matsushita Elec. Ind., Osaka, Japan, is used for a room air conditioner. The array detects the position and number of persons and their body temperatures to create a comfortable space (20,21).

Thin Film Optical Waveguide Devices

Thin film optical waveguide devices commonly consist of a sandwich structure of a thin film waveguide and a substrate. The refractive index of the thin film waveguide is larger than the substrate value so that a guided light beam propagates in the thin film waveguide. The direction of a propagated light beam is controlled by the channel waveguide shown in Fig. 12. The waveguide thin films comprise functional materials including EO or AO materials such as LN, PLZT, and ZnO. The PLZT thin films exhibit a linear EO effect or a quadratic EO effect depending on their composition. Typical EO properties of PLZT thin films are shown in Fig. 13. The birefringence shift $\delta\Delta n$ is several times larger than for conventional LN crystals. The linear EO coefficient r is given by the relation $\delta\Delta n = -\frac{1}{2} \times n^3 rE$ and the quadratic E/O coefficient R is given by the relation $\delta\Delta n = -\frac{1}{2} \times n^3 RE^2$, where n is the refractive index and E is the applied electric field. The value of R is 0.6×10^{-16} $(\mathrm{m/V})^2$ and r is 0.81×10^{-10} m/V. The light beam is introduced using an optical coupler such as a prism, micrograting coupler, and microlens directly connected to the optical fiber. The thin film waveguide is fabricated by deposition of the functional thin films on a substrate followed by microfabrication. The surface treatment such as doping of a foreign element on the functional crystal substrate (i.e., Ti doping on LN) is also used for the fabrication of thin film waveguides. Typical thin film waveguide devices are shown in Figs. 14–16.

Figure 14(a) shows the Mach–Zehnder interferometric modulator. The input light signal is equally divided into two waves by the branching guide and fed through two parallel arms of guide. In each arm, the waves are electro-optically modulated by the applied field. The intensity of guided light of TE_0 mode is strongly modulated because of a large EO effect. A typical sinusoidal pattern is observed as the applied electrical field is varied as shown in Fig. 14(b). The Bragg diffraction switches comprise PLZT epitaxial thin films on sapphire for the EO switch and ZnO epitaxial thin films on sapphire for the AO switch, respectively. The guided light, chiefly TE_0 mode, is diffracted as a result of a periodic grating with refractive index by applying a periodical electrical field for the EO switch using an interdigital electrode and by applying SAW for the AO switch using a interdigital SAW transducer. The angle of diffraction is governed by the Bragg diffraction, and the diffraction angle 2θ is given by $2\theta = \lambda_0/n\lambda_s$, where θ denotes the Bragg angle, λ_0 denotes the wave-

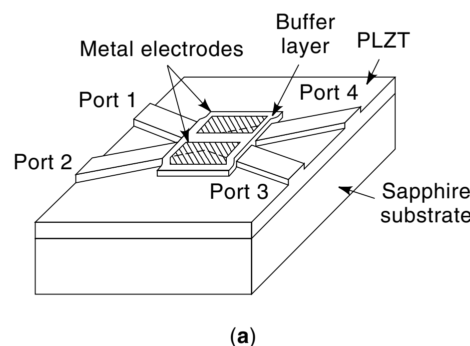

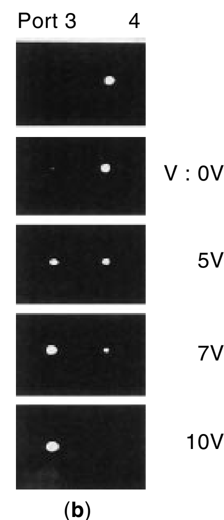

Figure 16. (a) Configuration of thin film TIR optical waveguide switch using PLZT thin film on sapphire and (b) the light intensity output at port 3 and 4 for various applied voltages (27).

length of light, n denotes the effective refractive index of the waveguide, and λ_s denotes the wavelength of the interdigital electrode. Figure 15 shows a typical operation of the ZnO thin film AO deflector. The Bragg deflector is driven by the first-order mode of SAW (Sezawa mode) with a phase velocity of 5700 m/s. The IDT is designed for 2 GHz operation. The TE_0 mode of a guided He—Ne laser beam is effectively deflected by the high-frequency SAW.

The total internal reflection (TIR) switch, which was first proposed by C. S. Tsai, is composed of a pair of crossed channel PLZT (20/0/100) waveguides, quadratic EO, with four terminals on sapphire as shown in Fig. 16(a). The intersecting angle of the channel waveguide θ satisfies the relation, $\theta < 90 - \theta_c$, $\theta_c = 1/\sin(1 - \frac{1}{2} n^2RE^2)$, where θ_c denotes the critical angle of total reflection, R denotes the quadratic EO coefficient, and E denotes the electrical field at the crossed area. At the crossed area, a pair of control electrodes are deposited to apply a control electrical field. Figure 16(b) shows a typical operation of the PLZT TIR switch. The TE_0 mode of the guided He—Ne laser beam directly coupled from port 1 propagates to port 3 without applying a control voltage, but the guided light is switched to port 4 as a result of the decreased refractive index at the interaction area under the application of control voltages. The switching voltage is less than 5 V due to the high EO coefficient of PLZT. The switching speed is expected to be as high as 100 GHz.

Thin film waveguide devices are flourishing. A number of promising devices are proposed for optical communication systems and integrated optical circuits, including optical computing (22–29).

BIBLIOGRAPHY

1. L. E. Cross, Ferroelectric ceramics. In N. Setter and E. L. Colla (eds.), *Ferroelectric Ceramics,* Berlin: Birkhauser, 1993.
2. G. H. Haertling and C. E. Land, Hot-pressed (Pb,La)(Zr,Ti)O_3 ferroelectric ceramics *J. Amer. Ceram. Soc.,* **54**: 1, 1971.
3. K. L. Chopra, *Thin Film Phenomena,* New York: McGraw-Hill, 1969.
4. G. H. Haertling, Ferroelectric thin films for electronic applications, *J. Vac. Sci. Technol.,* **A9** (3): 414, 1991.
5. R. F. Bunshah, *Deposition Technologies for Films and Coatings* Park Ridge, NJ, Noyes, 1982.
6. K. Wasa and S. Hayakawa, *Handbook of Sputter Deposition Technology,* Park Ridge, NJ, Noyes, 1992.
7. G. S. Kino and R. S. Wagers, Theory of interdigital couplers on nonpiezoelectric substrates, *J. Appl. Phys.,* **44**: 1480, 1973.
8. W. R. Smith et al., Analysis of interdigital surface wave transducers by use of an equivalent circuit model, *IEEE Trans. Microwave Theory Tech.,* **MTT-17** (11): 856, 1969.
9. S. Ono, K. Wasa, and S. Hayakawa, Surface-acoustic wave properties in ZnO-SiO_2-Si layered structure, *Wave Electron.,* **3**: 35, 1977.
10. G. W. Farnell and E. L. Adler, *Physical Acoustics,* Vols. 9, 35, New York: Academic Press, 1972.
11. K. Sezawa and K. Kanai, *Bull. Earth. Res. Inst. Tokyo,* **13**: 237, 1935.
12. F. S. Hickernell, DC triode sputtered zinc oxide surface elastic wave transducers, *J. Appl. Phys.,* **44**: 1061, 1973.
13. S. Ono et al., SAW resonators using rf-sputtered ZnO films on glass substrates, *Appl. Phys. Lett.,* **33**: 217, 1978.
14. K. Setsune et al., Preparation and application of ZnO thin film by cylindrical magnetron sputter—ZnO thin film SAW long delay line, *Jpn. J. Appl. Phys.,* **20**: 137, 1981.
15. K. L. Davis, Properties of the MZOS surface wave convolver configuration, *IEEE Trans. Electron Devices,* **ED-23**: 554, 1976.
16. F. Hickernell et al., An integrated ZnO/Si-MOSFET programmable matched filter, *IEEE Ultrason. Symp. Proc.,* 223, 1975.
17. T. Mitsuyu, O. Yamazaki, and K. Wasa, A 4.4 GHz SAW filter using a single-crystal ZnO film on sapphire, *1981 IEEE Ultrason. Symp. Proc.,* 74, 1983.
18. S. S. Eaton et al., A ferroelectric nonvolatile memory. *Tech. Dig. IEEE Int. Solid-State Circuit Conf.,* p. 130, 1988.
19. D. W. Bondurant and F. P. Gnadinger, Ferroelectrics for nonvalatile RAMS *IEEE Spectrum,* **26** (7): 30 1989.
20. W. Wersing, *Ferroelectric device.* In N. Setter and E. L. Colla (eds.), *Ferroelectric Ceramics,* Berlin: Birkhauser, 1993.
21. T. Kamada et al., Pyroelectric infrared sensors made of La-modified $PbTiO_3$ thin films and their applications, *Integrated Ferroelectrics,* **11**: 15, 1995.
22. C. E. Land, New devices using ferroelectric thin films, *Proc. Int. Electron Devices Meeting,* Washington, DC. Dec. 1989, p.10.1.1, 1989.
23. H. Adachi et al., Ferroelectric (Pb,La)(Zr,Ti)O_3 epitaxial thin films on sapphire grown by rf-planar magnetron sputtering, *J. Appl. Phys.,* **60**: 736, 1986.
24. D. Botez and G. J. Herskowitz, Components for optical communications systems, *Proc. IEEE,* **68**: 689, 1980.
25. T. Kawaguchi et al., Optical PLZT thin film waveguides, *Appl Opt.,* **20**: 2187, 1984.
26. C. S. Tsai, B. Kim, and F. Akkari, Optical channel waveguide switch and coupler using total internal reflection, *IEEE J. Quantum Electron.,* **QE-14**: 513, 1978.
27. K. Wasa et al., Optical TIR switches using PLZT thin-film waveguides on sapphire, *J. Lightwave Technol.,* **LT-2** (5): 710, 1984.
28. K. Setsune et al., Discrete frequency Bragg deflector in 2 GHz range using ZnO/sapphire substrate, *IEEE Ultrason. Symp. Proc.,* 467, 1983.
29. C. S. Tsai, Integrated acoustooptic and magnetooptic devices for optical information processing, *Proc. IEEE,* **84**: 853, 1996.

KIYOTAKA WASA
Yokohama City University
KENTARO SETSUNE
Matsushita Electric Industrial Co.

THIN FILMS, HTS.

See HTS FILM GROWTH.